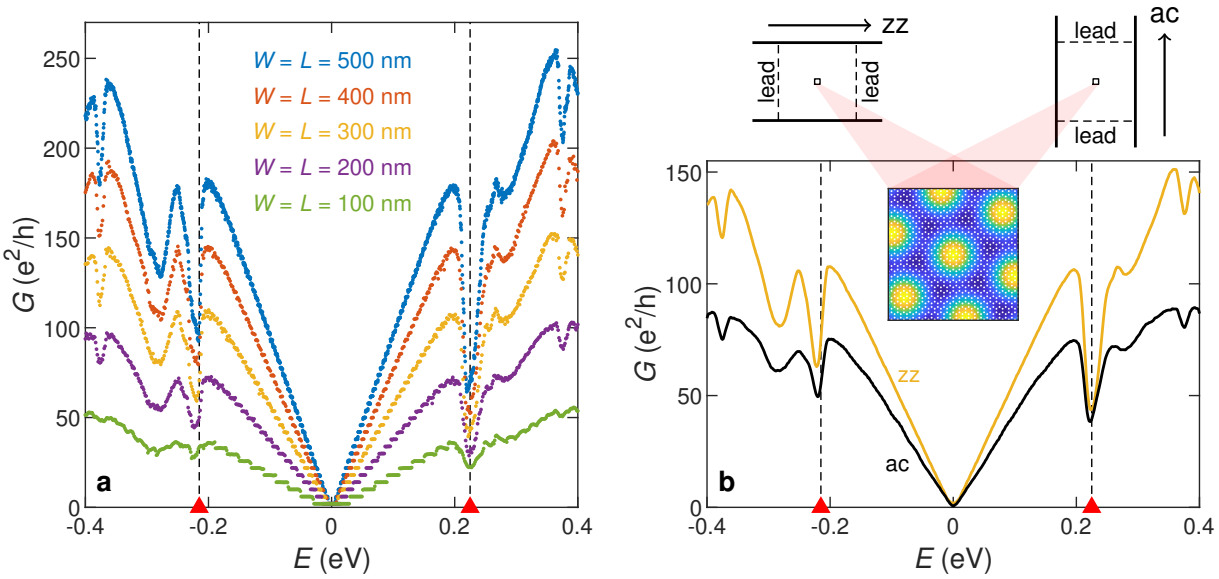

Supplementary Figure 1. **a** Conductance G as a function of Fermi energy E for a two-terminal device along the zigzag direction in the presence of the same $\phi = 0.9°$ moiré superlattice discussed in the main text, considering various sample sizes of length L and width W. The $W = L = 500\,\mathrm{nm}$ curve is exactly the same as Fig. 2**f** in the main text. **b** The yellow curve for a $W = L = 300\,\mathrm{nm}$ sample considers transport along the zigzag direction and is taken from the same data set shown in **a** with a moderate smoothing. With the same lattice and moiré superlattice potential, the black curve shows the conductance spectrum (also moderately smoothed) when attaching the leads in the vertical direction (see the sketches above), such that the transport is here along the armchair direction.

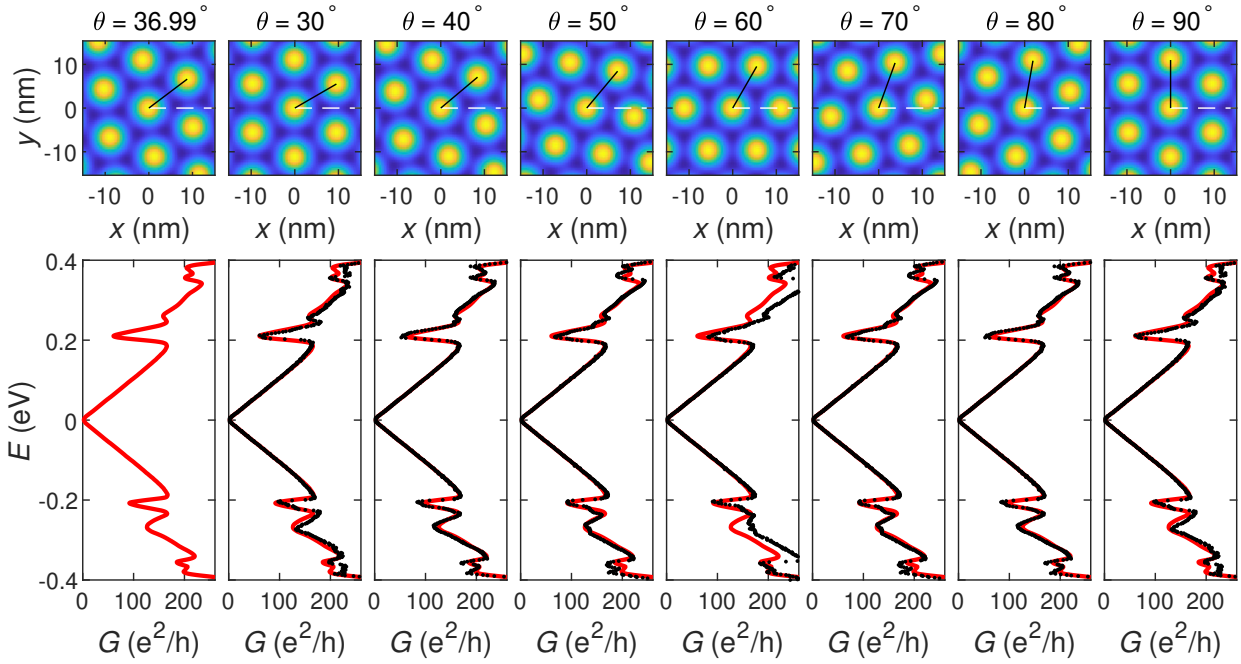

Supplementary Figure 2. Conductance G as a function of Fermi energy E for a $L = W = 500\,\mathrm{nm}$ two-terminal device (L and W being the length and width, respectively) along the zigzag direction in the presence of a moiré superlattice with periodicity $11\,\mathrm{nm}$, considering various moiré orientation angles θ. The leftmost column considers a realistic orientation angle θ obtained from Eq. (2) of the main text with fixed periodicity $\lambda = 11\,\mathrm{nm}$, which corresponds to a twist angle of $\phi = 0.7848°$. The obtained conductance curved (red) is shown as a reference for comparison in other panels, which consider the same moiré periodicity $\lambda = 11\,\mathrm{nm}$ but various orientation angle θ.

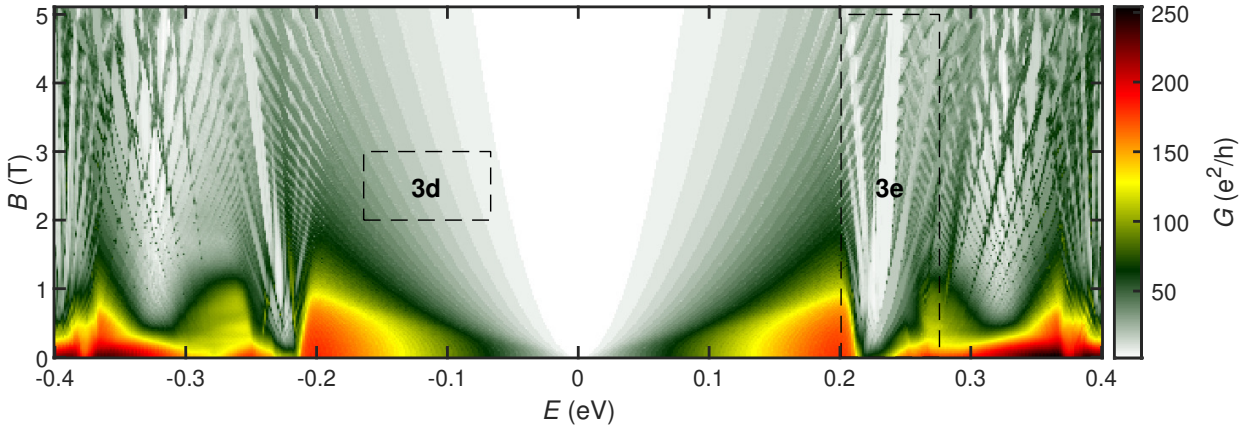

Supplementary Figure 3. Full map of the conductance G as a function of Fermi energy E and magnetic field B for the $L = W = 500\,\mathrm{nm}$ moiré superlattice device discussed in Fig. 3 of the main text (L and W being the length and width, respectively). The two dashed boxes mark the plot ranges corresponding to Figs. 3**d** and 3**e** of the main text, where the energy E dependence has been converted to the back gate V_{bg} dependence via Eq. (S1).

Supplementary Note 1. DEPENDENCE ON SAMPLE SIZE AND LATTICE ORIENTATION

In the main text, all simulations for the moiré superlattice are done by a $L = W = 500\,\mathrm{nm}$ two-terminal device with transport direction along zigzag. Here we show further calculations considering different sample sizes and compare the zigzag and armchair cases. In Supplemental Figure 1**a**, the two-terminal conductance as a function of Fermi energy is shown for various sample sizes. It can be seen that the conductance dips due to the moiré superlattice potential Eq. (1) emerges already at sample size as small as $100\,\mathrm{nm} \times 100\,\mathrm{nm}$, where quantized conductance steps within the ordinary Dirac cone energy range ($-0.2\,\mathrm{eV} \lesssim E \lesssim 0.2\,\mathrm{eV}$) can be seen. The locations of the secondary Dirac points marked by the red triangles and dashed black lines are clearly independent of the sample size.

Next, we further compare the two cases of zigzag and armchair, taking $L = W = 300\,\mathrm{nm}$ for an explicit example. The yellow curve shown in Supplemental Figure 1**b** are taken from panel **a** with a moderate smoothing, in order to better see the dip structures. Using the same lattice and moiré superlattice potential, but leads now attached in the vertical direction (see the sketches shown on top of Supplemental Figure 1**b**), the calculated conductance curve is shown as the black curve therein with the same moderate smoothing applied. Quite obviously, the conductance dips due to the emerging extra Dirac points remain the same. The overall drop of the conductance comes from the fact that the number of modes for the armchair case is slightly fewer than that of the zigzag case.

Supplementary Note 2. CONVERSION OF FERMI ENERGY TO GATE VOLTAGES

For our two-terminal device exhibiting the graphene/hBN moiré superlattice, we have converted the Fermi energy to the back gate voltage in the following way. First, we relate the back-gate-induced carrier density $n = (C/e)V_{\mathrm{bg}}$ with the Fermi energy through $E = \mathrm{sgn}(n)\hbar v_{\mathrm{F}}\sqrt{\pi|n|}$. These give us

$$V_{\mathrm{bg}} = \frac{e}{\pi C}\left(\frac{E}{\hbar v_{\mathrm{F}}}\right)^2 \mathrm{sgn}(E)\,, \tag{S1}$$

where C is the back gate capacitance per unit area given by the parallel-plate capacitance formula $C/e = (\epsilon_0/e)(d_{\mathrm{SiO_2}}/3.9 + d_{\mathrm{hBN}}/4.2)^{-1} \approx 6.77 \times 10^{10}\ \mathrm{cm}^{-2}V^{-1}$. Using this capacitance value, the exhibiting conductance dips at $V_{\mathrm{bg}} = +54.5$ V and -59.9 V observed in Fig. 2**d** correspond to

densities about $+3.7 \times 10^{12}$ cm^{-2} and -4.0×10^{12} cm^{-2}, respectively, so that the twist angle is estimated to lie in the range of $0.85° < \phi < 0.95°$. Indeed, when choosing $\phi = 0.9°$ for the moiré model potential Eq. (1), the simulated conductance $G(V_{\rm bg})$ transformed from $G(E)$ and reported in Fig. 2**e** is found to show excellent agreement with the experiment Fig. 2**d** in the positions of the conductance dips.

Supplementary Note 3. DEPENDENCE ON MOIRÉ ORIENTATION ANGLE

In the main text, we have modeled the moiré potential following Eq. (1) from Supplementary Ref. 1 (Ref. 3 of the main text) with the moiré pattern described by Eq. (2) following Supplementary Ref. 2 (Ref. 23 of the main text) where the orientation angle is defined with respect to the zigzag direction. In the following, we show that conductance dips revealed by the tight-binding transport simulations remain unchanged when the orientation angle θ is arbitrarily adjusted without following Eq. (2b).

We consider $L = W = 500\,\mathrm{nm}$ with transport along zigzag, in the presence of a moiré superlattice potential of periodicity $\lambda = 11\,\mathrm{nm}$, which corresponds to a twist angle of $\phi = -0.7848°$ according to Eq. (2a). The first (leftmost) column of Supplementary Figure **2** shows the "realistic case" as the reference, where the orientation angle $\theta \approx 36.99°$ follows from Eq. (2b). The same calculation is repeated with all parameters unchanged except the orientation angle adjusted to $30°, 40°, \cdots, 90°$, as shown in the rest of the columns in Supplementary Figure **2**, where the red reference curve is shown for comparison and the black dots are data points with various θ.

SUPPLEMENTARY REFERENCES

[1] Yankowitz, M. *et al.* Emergence of superlattice dirac points in graphene on hexagonal boron nitride. *Nat. Phys.* **8**, 382–386 (2012).

[2] Moon, P. & Koshino, M. Electronic properties of graphene/hexagonal-boron-nitride moiré superlattice. *Phys. Rev. B* **90**, 155406 (2014). URL https://link.aps.org/doi/10.1103/PhysRevB.90.155406.